Quantum Control of NaI Predissociation in Subpicosecond and Several-Picosecond Time Regimes

K. Hoki, Y. Ohtsuki,* H. Kono, and Y. Fujimura

Department of Chemistry, Graduate School of Science, Tohoku University, Aoba-ku, Sendai 980-8578, Japan

Received: March 15, 1999

Laser pulses that enhance the predissociation reaction of NaI are theoretically studied based on a local control method. Two control schemes corresponding to two time regimes, one of subpicoseconds and one of a few picoseconds, are considered. For subpicosecond control, the pulse is designed to induce the Tannor−Rice pump−dump scheme, in which an intrapulse pump−dump process is predicted. The created wave packet has a high velocity to accelerate the nonadiabatic transition because of the Landau−Zener mechanism. On a longer time scale (several picoseconds), we employ a two-step control scheme. First, we use a variational procedure to determine the target wave packet that has the shortest lifetime at a given time. Then we calculate the control pulse to shape this target by a backward time propagation technique. Numerical results show that the wave packets generated by the control pulses are effective for accelerating the predissociation of NaI.

1. Introduction

Application of femtosecond spectroscopy to NaI photodissociation dynamics enabled direct observation of a wave packet motion around a transition-state region.[1−5] These pioneering works stimulated experimental and theoretical studies on the control of NaI photodissociation using ultrafast tailored pulses.[6−9] One attempt[6] was to control the branching ratio between two channels of photodissociation products. The relevant potential energy surfaces (PESs) for this control involve ground-state ionic and covalent states as well as a higher lying neutral state in the diabatic representation. The former two potentials interact with each other around their crossing, which leads to the ground and excited adiabatic states. The first excited adiabatic state is unstable because it is nonadiabatically coupled to the ground state. Thus, the wave packet created on the first excited PES predissociates to the ground state to form ground-state Na and I atoms. On the other hand, the PES of the higher lying neutral state corresponds asymptotically to the product of the excited-state sodium atom Na*. In the experiment by Herek et al.,[6] a pump pulse prepares a wave packet on the first excited PES (Na+I product state), and then a control pulse partially removes this evolving wave packet to the highest PES (Na*+I product state). Since the control pulse is tuned to cause the second transition at a particular internuclear distance, change in the delay time between the two pulses can alter the branching ratio. They showed that an appropriate choice of the delay time achieved an Na/Na* branching ratio of about five.

The control scheme used in the study by Herek et al. relies on the fact that the localized wave packet is excited to the third state at a position which is specified by the frequency of the control pulse. Thus, a wave packet with a narrower spatial distribution can improve the energy resolution and is more efficiently promoted to the highest state, which results in high selectivity. For wave packet shaping, Wilson's group theoretically predicted and then experimentally observed that negatively chirped pulses can squeeze the spatial distribution width of an incoming (quasi) bound wave packet of I_2 molecules.[10−12] Recently, Bardeen et al.[8] applied these ideas to NaI photodissociation control. They generated a localized wave packet on the first excited PES using a negatively chirped pump pulse and then irradiated a Fourier transform-limited second pulse with an appropriate delay time to improve the branching ratio of the photodissociation products. Although their numerical simulation showed that the negatively chirped pump pulse enhanced the selectivity at 0 K, this effect was considerably diminished by thermal distribution at 1000 K and the latter result was confirmed experimentally. For a wave packet with sufficient outgoing momentum, Tang and Rice[9] recently pointed out that a positively chirped pulse sharpens its spatial distribution more efficiently than a negatively chirped pulse.

In this study, we design control pulses that accelerate the predissociation of NaI based on a local control method.[13−21] Generally, in polyatomic molecules, predissociation competes with other processes such as IVR or with other relaxation processes. Thus, it is important to analyze how to accelerate the predissociation reaction using a simple molecule such as NaI. For this purpose, we consider two control schemes, corresponding to two time regimes. One of them is based on the Tannor−Rice pump−dump[13,22−24] scheme for a subpicosecond time regime. In few-picoseconds control, we employ a two-step control method in which pulses generate a wave packet consisting of short-lived vibronic states in the predissociation well.[25,26] For this purpose, a backward time-propagation technique developed in our previous paper is applied to shaping this nonstationary target.[21]

Using a model diatomic system with three PESs, a similar control scheme based on the optimal control theory[13,27−33] was studied by Gross, Neuhauser, and Rabitz.[27] In this model, the lowest bound state is radiatively coupled to two excited repulsive states which interact with each other as a result of a nonadiabatic coupling. Starting with an initial wave packet on one of the excited states, optimal control theory is used to calculate the control pulses that dissociate the molecule through one of the dissociation channels.

In section 2, we briefly summarize our local control method. Our numerical procedure and the potential parameters of NaI

10.1021/jp990894d CCC: $18.00
Published on Web 07/27/1999

are also introduced. In section 3, we present calculations of local control pulses based on the above-mentioned two control schemes.

2. Theory

A. Local Control Pulse.[20,21] Consider a molecule interacting with a time-dependent electric field $E(t)$, through an electric-dipole interaction, whose Hamiltonian is given by

$$H^t = H_M + V^t = H_M - \mu E(t) \tag{1}$$

where H_M, V^t, and μ are a molecular Hamiltonian, an interaction Hamiltonian, and an electric dipole moment operator, respectively. This molecular system obeys the Schrödinger equation

$$i\hbar\frac{\partial}{\partial t}|\psi(t)\rangle = H_M|\psi(t)\rangle - \mu\, E(t)|\psi(t)\rangle \tag{2}$$

We first introduce a target operator W, which gives a maximum expectation value when a molecule reaches an objective state. Then the optimal control pulse is determined so as to maximize the expectation value at a control time t_f, while minimizing the pulse energy. Mathematically, the optimal control pulse thus leads to an extremal value of the following objective functional:

$$J[E(t)] = \langle W(t_f)\rangle - \frac{1}{\hbar A}\int_{t_0}^{t_f} dt[E(t)]^2 \tag{3}$$

where the second term represents the penalty due to the pulse energy. Here, the positive constant A weights the significance of it. The constraint originating from the Schrödinger equation (eq 2) is included through the time-evolution operator. Equation 3 can be written as

$$J[E(t)] = \int_{t_0}^{t_f} dt\left\{\frac{d}{dt}\langle W(t)\rangle - \frac{1}{\hbar A}[E(t)]^2\right\} + \langle W(t_0)\rangle \tag{4}$$

If we assume that the integrand in eq 4 is given by a known function of time, $g(t)$, then

$$\frac{d}{dt}\langle W(t)\rangle - \frac{1}{\hbar A}[E(t)]^2 = g(t) \tag{5}$$

and we can therefore determine the pulse shape locally in time. This is our basic idea behind the design of a local control pulse.[21] Since the function $g(t)$ specifies the path in the functional space a priori, our control pulse satisfies the equation $\delta J = 0$, although it cannot be simply equated with the necessary condition of an optimal control pulse.

Here, we are concerned with the special case where the function $g(t)$ is chosen as

$$g(t) = 0 \tag{6}$$

This path requires that the penalty due to the pulse energy should be canceled by the increase in the target expectation value. In this case, we obtain the condition of a commutation relation

$$[H_M, W] = 0 \tag{7a}$$

or more correctly speaking

$$\langle\psi(t)|[H_M, W]|\psi(t)\rangle = 0 \tag{7b}$$

Thus, eq 5 is reduced to

$$E(t)\{E(t) - iA\,\langle\psi(t)|[W, \mu]|\psi(t)\rangle\} = 0 \tag{8}$$

Since the solution $E(t) = 0$ is allowed only in the trivial case of starting out in the objective state, the local control pulse is expressed as

$$E(t) = -2AIm\{\langle\psi(t)|W\mu|\psi(t)\rangle\} \tag{9}$$

In the present study, we restrict ourselves to this special case and use eq 9 to design the control pulses.

The approximate solution, eq 9, can be interpreted from another viewpoint, which directly connects it with an optimal solution. Recently, Zhu et al.[34−36] proposed a novel rapid convergent algorithm to efficiently solve the control equations derived from the same objective functional as eq 3. If we assume a null electric field as a zero-order solution (initial guess), then we can obtain eq 9 at a first iteration step of their calculation scheme. Thus, eq 9 can be regarded as the lowest-order iterative solution to the optimal control problem. Since their algorithm generally shows a very rapid convergence behavior, we may say that eq 9 gives a good approximate solution in a wide range of applications.

Finally, we emphasize again that there is a restriction originating from the commutation relation eq 7a when we use eq 9 to design a control pulse. This condition prevents us from achieving nonstationary objectives with the direct application of eq 9. To overcome this difficulty, we showed that an appropriate choice of a target operator together with the backward time-propagation technique can make it possible to control nonstationary states such as wave packet dynamics.[21] In the present study, we employ this technique to design a control pulse that generates target wave packets.

B. Numerical Calculation. The molecular Hamiltonian H_M is written as the sum of a nuclear kinetic energy operator, $\hat{T}_n$, and an electronic part, $\hat{H}_{el}$

$$H_M = \hat{T}_n + \hat{H}_{el} \tag{10}$$

where $\hat{H}_{el}$ includes the kinetic energy of electrons, electron−electron interactions and electron−nuclei interactions. For numerical calculation,[37−39] we introduce a diabatic basis set $\{|d(R)\rangle\}$ in which the quantum number d specifies the diabatic electronic state, and R in the parentheses indicates its parametric dependence on nuclear coordinates. The Schrödinger equation expanded in terms of the basis $\{|dR\rangle = |d(R)\rangle|R\rangle;\ |R\rangle$ is an eigenvector of the nuclear coordinate$\}$ is given by

$$i\hbar\frac{\partial}{\partial t}\phi_d(R,t) = \int dR_1\,\langle R|\hat{T}_n|R_1\rangle\phi_d(R_1,t) + \sum_{d_1}[V_{dd_1}(R) - \mu_{dd_1}(R)E(t)]\phi_{d_1}(R,t) \tag{11}$$

since the matrix element of the nuclear kinetic operator has a form of

$$\langle dR|\hat{T}_n|d_1R_1\rangle = \langle R|\hat{T}_n|R_1\rangle\delta_{dd_1} \tag{12}$$

Here, $\phi_d(R,t) = \langle dR|\psi(t)\rangle$ represents a nuclear wave packet on the dth diabatic state. The matrix element $V_{dd_1}(R)$ is defined by

$$V_{dd_1}(R) = \int dR_1\,\langle dR|\hat{H}_{el}|d_1R_1\rangle = \langle d(R)|\hat{H}_{el}(R)|d_1(R)\rangle \tag{13}$$

where $\hat{H}_{el}(R)$ is the electronic operator in the coordinate representation of nuclei. The matrix element of the transition moment operator $\mu_{dd_1}(R)$ is defined by an expression similar to eq 13. To numerically integrate eq 11, we divide the

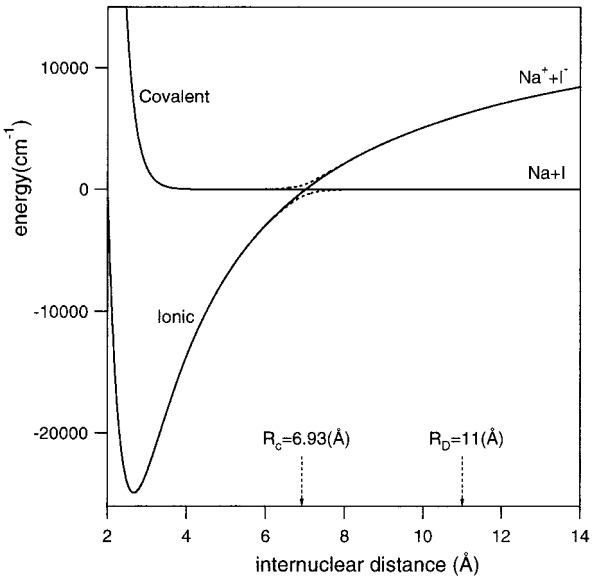

Figure 1. Potential energy surfaces (PESs) for NaI. The solid (dotted) lines represent the diabatic (adiabatic) PESs, whose parameters are taken from ref 39. The diabatic potentials cross at $R_c = 6.93$ Å. When the wave packet components on the covalent diabatic state have a nuclear separation larger than $R_D = 11.0$ Å, they are regarded as dissociation products.

Hamiltonian into kinetic and potential operators according to the split-operator + FFT (fast Fourier transform) scheme.[37,39−42] The potential couplings due to diabatic interactions and optical transitions are calculated using the Pauli matrix.[27] When we need a wave packet on an *a*th adiabatic electronic state $|a(R)\rangle$, we can obtain it using a transformation function[37] $\Lambda_{da}(R) = \langle d(R)|a(R)\rangle$

$$\phi_a(R,t) = \sum_d \Lambda^*_{da}(R)\phi_d(R,t) \tag{14}$$

The adiabatic potential $V_a(R)$ and $\{\Lambda_{da}(R)\}$ are determined by the eigenvalue equation

$$\sum_{d_1} V_{dd_1}(R)\Lambda_{d_1a}(R) = V_a(R)\Lambda_{da}(R) \tag{15}$$

whose coefficient matrix is given by the diabatic potential elements $\{V_{dd_1}(R)\}$.

In this paper, we adopt a two-electronic-surface model that consists of ground-state ionic $\{|d_i(R)\rangle\}$ and covalent states $\{|d_c(R)\rangle\}$ (in a diabatic representation). Their potential parameters were taken from ref 39, although they were originally published in refs 43−45. The PESs are illustrated in Figure 1. To avoid artificial reflection of a wave packet at a boundary, we add an optical potential on each potential. Our control pulses are designed to interact with NaI only when the wave packets are around the Franck−Condon region with the lowest state. Thus, the matrix elements of the dipole operator are assumed to be independent of the nuclear separation, and its value was chosen as 1.0 Debye. We use the calculation range of $R \in [R_{\min} = 1.0$ Å, $R_{\max} = 23.0$ Å] with 2048 grid points and a time grid size of $\Delta t = 2.0 \times 10^{-2}$ fs. The time- and frequency-resolved spectrum $S(\omega,t)$ of a control pulse $E(t)$ is calculated by

$$S(\omega,t) = |\int_{-\infty}^{\infty} d\tau H(\tau - t, T_w)E(\tau)\, e^{i\omega\tau}|^2 \tag{16}$$

using the Blackman window function $H(\tau - t, T_w)$. This function

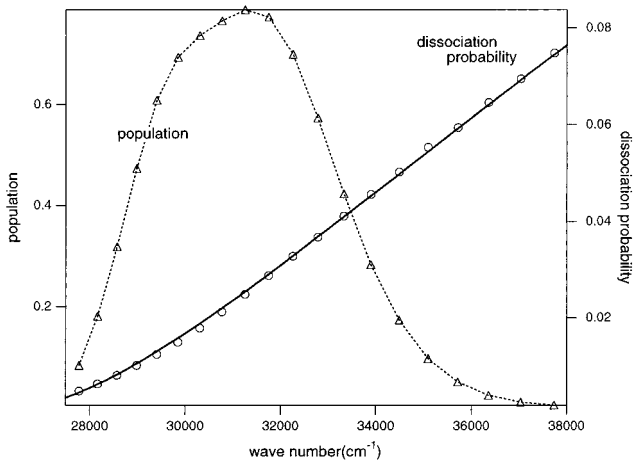

Figure 2. The excitation population (triangles with dotted line) and dissociation probability (circles) as a function of photon energy of the pulse. The definition of the dissociation probability is given in the text. The excitation pulse has an envelope function of a 60 fs Gaussian with a peak intensity of 3.0×10^9 V/m. The solid line shows the dissociation probability fitted to the Landau−Zener formula using least- squares fitting.

is given by

$$H(\tau, T_w) = 0.42 + 0.50\cos\left(\frac{2\pi}{T_w}\tau\right) + 0.08\cos\left(\frac{4\pi}{T_w}\tau\right) \tag{17}$$

with time resolution T_w when $|\tau| \le T_w/2$, and is set to zero when $|\tau| \ge T_w/2$.

To numerically check the features of the potential energy surface (PES) adopted here, we calculate the excited population and dissociation probability when NaI is excited by a 60 fs Gaussian pulse.[6] This pulse has a fixed peak intensity of 3.0×10^9 V/m, while its central frequency is changed from 28000 cm^{-1} to 38000 cm^{-1}. In our calculation, wave packet components on the covalent PES that have nuclear separation larger than $R_D = 11.0$ Å are regarded as dissociation components, Na+I (Figure 1). Since the diabatic potentials cross each other around a nuclear separation of 6.9 Å, the nonadiabatic interaction can be negligible beyond the distance R_D. Figure 2 shows the population excited from the ground state and the dissociation products created through the first passage of the wave packet at the curve crossing. For the sake of normalization, the dissociation probability is given by dividing the dissociation components by the excited population. We can see that the excited population increases and then decreases as a function of frequency of the excitation pulse, reflecting the magnitude of the Franck−Condon factors. On the other hand, an increase in the excitation energy monotonically raises the dissociation probability. This is because a pulse with a higher frequency can generate a wave packet with a higher velocity at the crossing point that accelerates the nonadiabatic transition, i.e., predissociation. In Figure 2, this Landau−Zener mechanism is confirmed by the agreement between the calculated results and those fitted by the Landau−Zener formula.[46]

3. Results and Discussion

A. Pump−Dump Excitation Scheme. The Landau−Zener predissociation mechanism[46] suggests that a wave packet with a higher velocity can cause nonadiabatic transitions more efficiently and can accelerate the predissociation. As shown in Figure 2, however, the optical transition is limited by the restriction because of the Franck−Condon factors, which makes

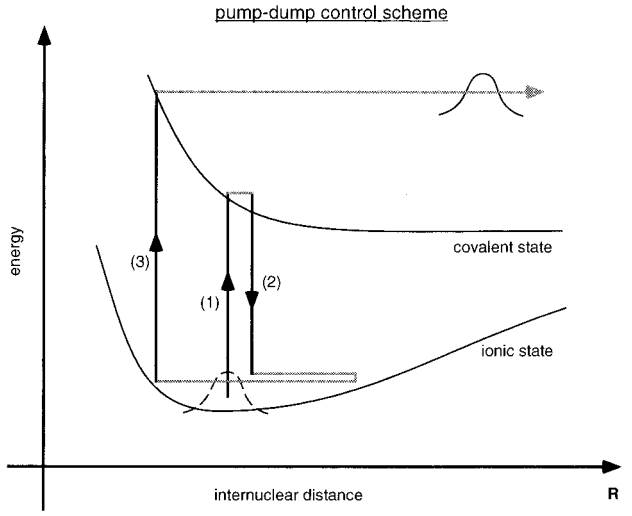

Figure 3. Schematic illustration of a pump−dump control. The solid lines with arrows indicate the first pump (1), dump (2), and second pump (3) processes. The thin lines trace the wave packet motion on each PES.

it difficult to generate this packet using a simple one-pulse excitation. To overcome this difficulty, we adopt a pump−dump excitation scheme,[13,22−24] which is illustrated in Figure 3. In this scheme, a first pump pulse (pulse 1) generates a wave packet on the excited PES. When the excited packet moves down the PES and reaches an appropriate region, it is transferred back to high vibrational states in the ground PES by a dump pulse (pulse 2). This packet oscillates within the ground PES with a large amplitude. When this packet reaches the inner turning point, it is pumped up to the excited PES again by a second pump pulse (pulse 3). Since a packet that has a large amplitude at a short nuclear distance can have large Franck−Condon factors with high vibrational states in an excited PES, a newly formed packet can possess a higher velocity at the curve crossing than a packet created by the first pump pulse.

According to this control scheme, we construct the following target operator W. Before doing so, we introduce vibronic states $\{|iv\rangle\}$, which are vibrational eigenstates in the ground PES and are obtained by diagonalyzing the molecular Hamiltonian H_M. The electronic parts of these states are well-characterized by the ionic state, and we therefore denote them as $\{|iv\rangle\}$ with a vibrational quantum number v. Since the first pump and dump pulses are well-separated from the second pulse in time, we use the target operator of

$$W = \sum_{v=0}^{9} |iv\rangle\, w_v\, \langle iv| \tag{18}$$

for $0 \le t \le 100$ fs and

$$W = H_M + \sum_{v=0}^{9} |iv\rangle\, w_v\, \langle iv| \tag{19}$$

for 100 fs $\le t \le$ 140 fs. Here, we do not specify the states with a quantum number greater than 9 since it is hard to optically control such states because of the small Franck−Condon factors. In eq 19, H_M is a molecular Hamiltonian, whose energy is measured in units of cm^{-1}. Corresponding to this choice of energy unit, the weight factors $\{w_v\}$ are also measured in units of cm^{-1}. The units for electric fields are set to V/m and are adjusted by an appropriate choice of units for the amplitude parameter A in eq 9. In eq 18, the weight factors are chosen as

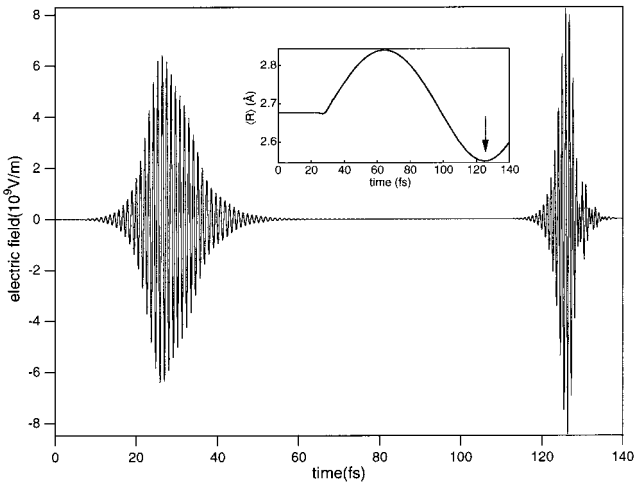

Figure 4. Designed pulses as a function of time. The first pulse around $t = 25$ fs corresponds to the first pump and dump processes (intrapulse pump−dump mechanism). The second pulse around $t = 128$ fs transfers the wave packet in the ground PES to the excited state. The temporal peak of the latter pulse coincides with the time when the packet reaches the inner turning point. This is indicated by the arrow in the inset which shows the averaged position of the packet as a function of time.

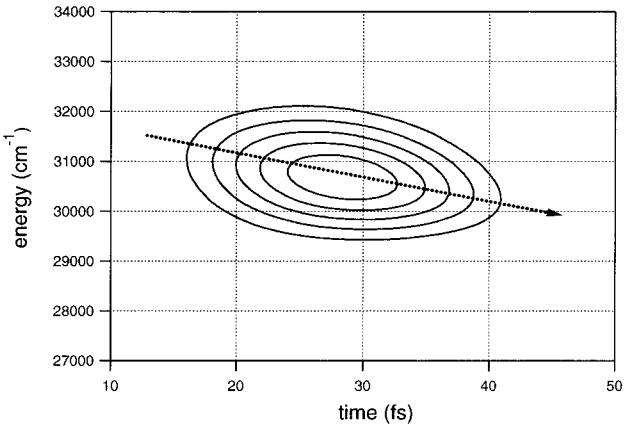

Figure 5. Time- and frequency-resolved spectrum (eqs 16 and 17) of the first pump and dump pulses in Figure 4. The time-resolution of the window function is chosen as $T_w = 50$ fs. The dotted line with an arrow indicates almost linear chirping.

$w_0 = -150$ cm^{-1}, $w_1 = 0$ cm^{-1}, and $w_v = 200$ cm^{-1} ($v \ge 2$), and in eq 19, they are set to $w_v = 6300$ cm$^{-1} - \epsilon_v$, where ϵ_v is an energy eigenvalue of the state $|iv\rangle$. The threshold energy, 6300 cm^{-1}, is introduced to avoid populating the low-energy states on the excited PES. For the amplitude parameter, $A = 9.94 \times 10^7$ and $A = 5.27 \times 10^6$ are used for the time ranges of $0 \le t \le 100$ fs and 100 fs $\le t \le$ 140 fs, respectively.

The calculated control pulse is shown in Figure 4, in which the average nuclear distance of the packet in the ground state is given in the inset. The first pump and the dump pulses form one pulse, which causes pump and dump processes sequentially in time. Since these processes occur at a slightly different nuclear separation, they have slightly different transition frequencies. In this case, the dumping requires a lower frequency than does the pumping, and the pulse is therefore a negatively chirped pulse.[27,47−51] The time- and frequency-resolved spectrum in Figure 5 clearly shows that the pulse is one of linear chirping. This chirping mechanism can be understood on the basis of the semiclassical description of the wave packet motion.[50,51] The numerical results show that the packet created by this control pulse has a 530 cm^{-1} higher average vibrational energy than

the initial state. To semiquantitatively interpret this, we solve the Newton equation $m dv/dt = F_0$, where m is a reduced mass, v is a velocity of the center of the packet, and the force F_0 is approximated by $-dV_{ii}(R)/dR|_{R_0}$ with an equilibrium distance R_0.[52] If we assume that $v(t = 0) = 0$ at the excitation time and estimate the pulse temporal width at $\tau = 5$ fs, then the kinetic energy gained through the classical motion is given by $\Delta T = (F_0\tau)^2/2m = 550$ cm^{-1} which agrees with the numerical result. Since in our system, the excited PES has a steep slope around the Franck−Condon region, the intrapulse pump−dump process efficiently generates a wave packet with a large amplitude in the ground-state PES.

According to the next pump−dump process, the wave packet is excited to the upper PES again when it reaches the inner turning point with about a 100 fs time lag after the first pulse. The timing of this second pump pulse is closely correlated with the packet motion, as shown in the inset of Figure 4. The energy of the resulting packet is so high that about 10% of the packet directly dissociates to form Na^+ and I^- ions. To see how much this control scheme can enhance the dissociation probability defined in Figure 2, we compare it to that in the case of a 60 fs pulse with a central frequency of 31250 cm^{-1} (absorption maximum). The dissociation probability is 2.84 times larger than that of the latter. As can be seen in Figure 2, the 60 fs pulse with a central frequency of 38000 cm^{-1} can achieve almost the same dissociation probability as that of the control pulse. However, the former optical transition is nearly forbidden because of the negligibly small Franck−Condon factors, and only a very small fraction of population is therefore excited by this pulse. Contrary to this, the calculated control pulse excited 41% of the population. Thus, it is concluded that the pump−dump control scheme can considerably accelerate the predissociation reaction within 100 fs.

In the above calculation, the local control method showed the intrapulse pump−dump excitation process to generate a wave packet with a large amplitude. It should be emphasized that this is obtained without employing physical intuition. Experimentally, the importance of the intrapulse pump−dump process has been demonstrated by Shank's group[53,54] in dye molecules. Since we saw the same mechanism in a very different system, the intrapulse mechanism can be regarded as a common excitation technique for creating various wave packets and for controlling other molecular processes. In fact, such examples were recently reported by Cao, Wilson, and co-workers.[50,51] In one of the papers,[50] they proposed a new population inversion scheme, named molecular π-pulse, by combining a positive chirp effect with adiabatic passage technique.

B. Control Scheme for a Longer Time Scale. If we are concerned with a predissociation yield on a longer time scale, e.g., a few picoseconds, the control scheme based on the Landau−Zener mechanism does not always offer effective means. This is because the packet with a higher energy has a longer oscillating period and has fewer chances to pass the curve crossing compared to that with a lower energy. Thus, we have to adopt another control scheme to improve the dissociation yield in several picoseconds. For this purpose, we must consider interference effects to create a wave packet with the shortest lifetime in order to accelerate the dissociation yield.

Our scheme consists of two parts, as shown in Figure 6. In the first step, we determine the target wave packet that gives the maximum product yield at a given time $t = t_P$. In the second step, we design the control pulse that generates this target packet. If we assume that a target packet $|\psi(t_f)\rangle = |\psi_f\rangle$ is prepare by a control pulse at time $t = t_f$, then the survival probability S (remaining in the bound states) at t_p is given by

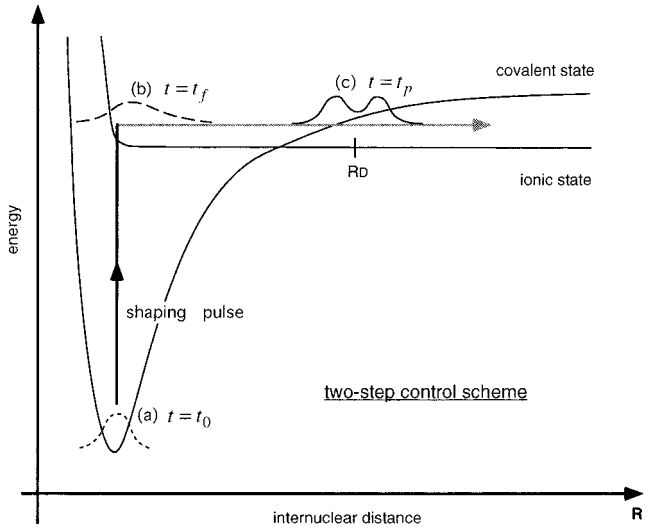

Figure 6. Schematic illustration of two-step control in a longer time (a few picoseconds) regime. The control pulse excites the initial packet [(a) $t = t_0$] to shape the target packet [(b) $t = t_f$], which is determined to give the maximum dissociation product at time t_P [(c) $t = t_P$]. The wave packet propagates freely for the time interval $t_P - t_f$. In our two-step control scheme, these processes are calculated inversely in time (see the text for details).

$$S = \frac{\langle\psi_f|U_0^\dagger(t_P,t_f)BU_0(t_P,t_f)|\psi_f\rangle}{\langle\psi_f|\psi_f\rangle} \tag{20}$$

where the free propagator is defined by

$$U_0(t_P,t_f) = \exp\left[-\frac{i}{\hbar}H_M(t_P - t_f)\right] \tag{21}$$

and the projector B for the bound components is expressed as

$$B = \int_{R_{\min}}^{R_{\max}}|iR\rangle dR\langle iR| + \int_{R_{\min}}^{R_D}|cR\rangle dR\langle cR| \tag{22}$$

Since we are now aiming at minimizing the survival probability S to enhance the predissociation at time t_P, we can determine the target packet according to a conventional variational procedure. The minimization of survival probability is equivalent to the maximization of dissociation probability; however, we employ the former target to avoid dealing explicitly with the optical potential. Before proceeding with our calculation, it should be noted that the target packet $|\psi_f\rangle$ is generated by a control pulse in the second step, and it must therefore be optically connected with the initial state. This leads to the constraint that the target packet is within a subspace of optically accessible states specified by a projector P:

$$P|\psi_f\rangle = |\psi_f\rangle \tag{23}$$

Under this constraint, we can derive the following eigenvalue equation from eq 20

$$P\,U_0^\dagger(t_P,t_f)B\,U_0(t_P,t_f)P|\psi_f\rangle = \lambda P|\psi_f\rangle \tag{24}$$

In our model, the nonadiabatic interaction is so weak that the vibrational states in the excited adiabatic PES $\{|a_2\ v\rangle,\ v = 0, 1, 2, \cdots\}$ offer an appropriate basis to represent the projector P. By this choice of the basis, we have

$$P = \sum_{v=v_{\min}}^{v_{\max}}|a_2\ v\rangle\langle a_2\ v| \tag{25}$$

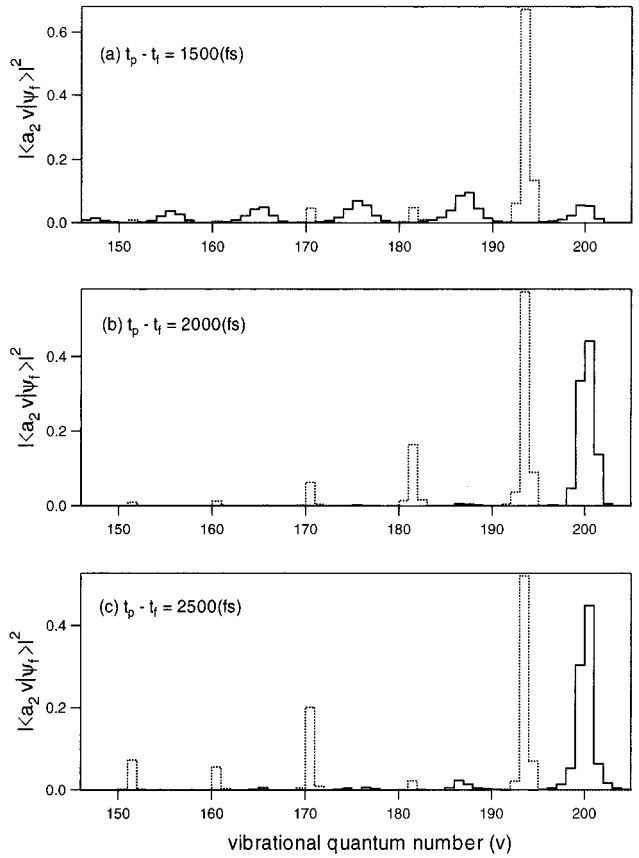

Figure 7. Vibrational-state distributions of the targets for several time intervals, (a) $t_P - t_f = 1500$ fs, (b) $t_P - t_f = 2000$ fs, and (c) $t_P - t_f = 2500$ fs. Those of the packets with the largest survival probabilities are also shown by dotted lines.

where v_{min} and v_{max} are determined by the magnitude of the Franck−Condon factors. That is, we only include vibrational states that have Franck−Condon factors greater that 0.007, whereby they are set to $v_{min} = 146$ and $v_{max} = 205$. Substituting eq 25 into eq 24, all of the matrix elements are calculated by the time propagation method starting with each vibrational state. We then solve eq 24 by a diagonalization method to obtain the target packet which is the eigenstate with the minimum eigenvalue.

In Figure 7, the vibrational-state distributions of the targets for several time intervals of $t_P - t_f$ are shown by solid lines. For comparison, those of the eigenstates with the largest survival probability are shown by dotted lines. Comparing the results, we can see that the vibrational states exhibit different distribution patterns; i.e., in each figure of Figure 7, the vibrational states included in one of the packets do not appear in the other. This can be understood on the basis of the lifetime of the vibrational states employed here (eq 25). The vibrational state with a short lifetime considerably predissociates before time t_P, and it therefore makes only a small contribution to the matrix elements of the bound-state projector B. Thus, the target packet with the minimum eigenstate mainly consists of these short-lifetime states. Contrary to this, the eigenstate with the maximum eigenvalue includes only the vibrational states with a long lifetime. Another factor determining the target shape is the number of times the target packet has a chance to pass the curve crossing with an outgoing momentum. Thus, the eigenstates with large survival probabilities tend to include high vibrational states with a long lifetime in order to prolong the oscillating periods, and their phases are adjusted to have inner momenta. To see the latter trend of the phase effects, we consider the target packet

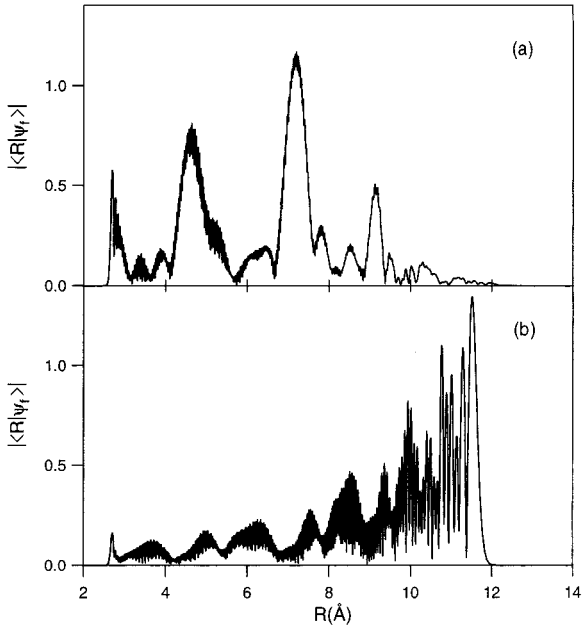

Figure 8. Absolute values of the wave packets as a function of internuclear separation R for (a) the target packet and (b) the packet with the largest survival probability at the time interval $t_f - t_P = 1500$ fs [Figure 7(a)].

given in Figure 7(a). Figure 8(a) shows the absolute value of this target packet as a function of nuclear separation. Since this packet has an eigenvalue of $\lambda_{min} = 0.859$, 14.1% of it dissociates within $t_P - t_f = 1500$ fs after the optical preparation. For comparison, the packet with the largest eigenvalue ($\lambda_{max} = 0.998$) is shown in Figure 8(b). This eigenvalue means that 99.8% of the packet created at time t_f can survive without dissociation for $t_P - t_f = 1500$ *f*s. The target packet in Figure 8(a) localizes around $R \in$ (2.6 Å, 9.5 Å) and has a positive average momentum. We see that the largest component is designed to pass the crossing point just after t_f. Contrary to this, in Figure 8(b) the distribution of the packet with the longest lifetime extends far beyond the crossing point, and the packet starts to move toward the inner potential region after the preparation time t_f. Thus, its shape is determined to avoid passing the crossing point within $t_P - t_f = 1500$ fs. In general, the lifetime and phase effects compete with each other, and the vibrational-state distributions of the target packets have different patterns, as can be seen in Figure 7.

We now move on to the second step in designing the control pulse for generating the target packet. To deal with the nonstationary target state in the local control method, we have to utilize a backward propagation technique.[21] In this method, the pulse shape is determined so as to transfer the target packet to the lowest state inversely in time. Then we substitute the calculated pulse back to the Schrödinger equation forward in time to ascertain whether it really controls the dynamics. There are two methods of backward propagation treatment.[21] One of them starts with the target packet and maximizes the yield of the lowest state. In the other, we adjust the target population and find the pulse that completely transfers the population to the lowest state. In both cases, the achievement obtained in backward propagation can be proven to be the same as that in forward propagation because of the time reversibility of the Schrödinger equation. In this study, we adopt the latter method and employ the 1:1 superposition state of the target packet and the lowest state instead of the pure target packet. This means that the calculated pulse controls 50% of the population. That is, the control pulse transfers half of the population from the

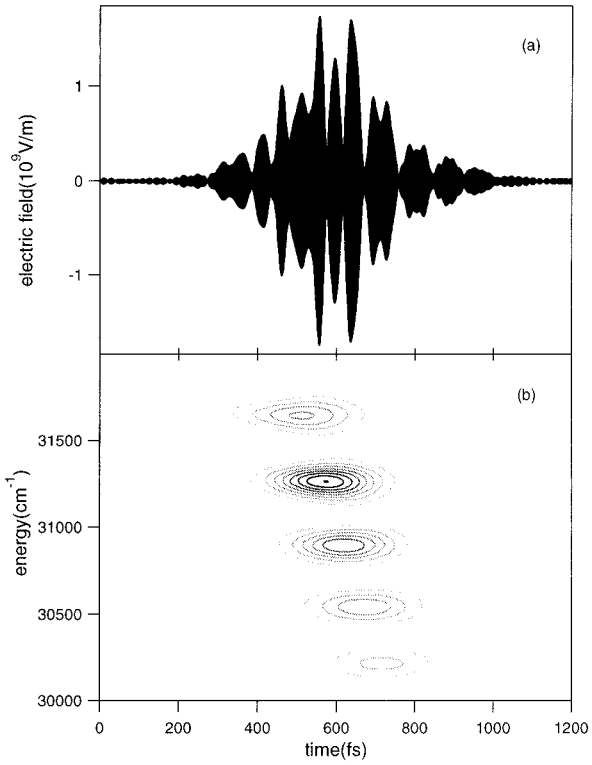

Figure 9. Calculated control pulse for shaping the target packet in Figure 8(a). The control pulse as a function of time (a) and its time- and frequency-resolved spectrum (b). In (b), the time-resolution of the window function is chosen as $T_w = 300$ fs.

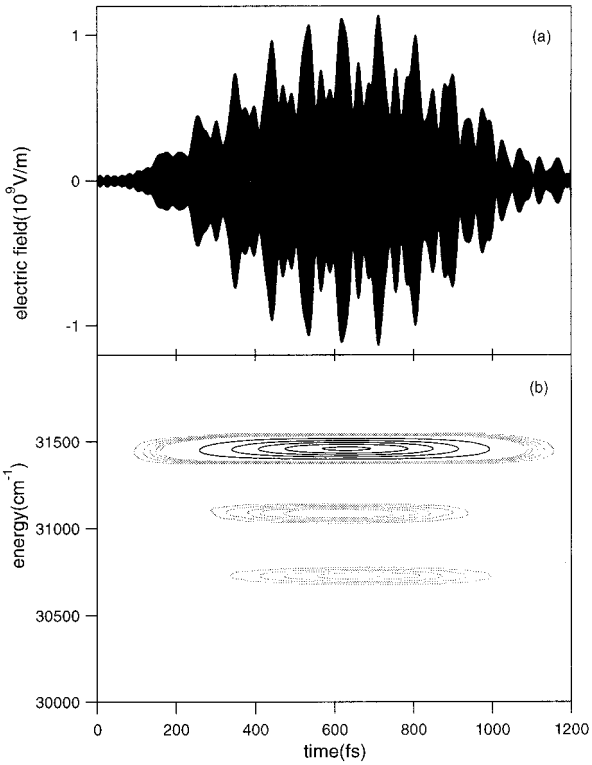

Figure 10. Calculated control pulse for shaping the target packet in Figure 8(b). The control pulse as a function of time (a) and its time- and frequency-resolved spectrum (b). In (b), the time-resolution of the window function is chosen as $T_w = 700$ fs.

lowest state to the target packet, and the other 50% of the population remains in the lowest state. We numerically checked that the phases of two states in the superposition state do not change the shape of the control pulse.

In the backward propagation, the target state is the lowest state, which is represented by $|iv=0\rangle$ using the notation introduced in eq 18. Thus, we use the target operator that has the form of

$$W = \sum_{v=0}^{v_{max}} |iv\rangle\, w_v\, \langle iv| \tag{26}$$

where the weight factors are chosen as $w_0 = 1.0$ and $w_v = -0.1$ with $v_{max} = 7$. The latter negative weights are a penalty that prevents the pulse from populating the vibrationally excited states. To shape the packets in Figure 8(a) and (b), the amplitude parameters are chosen as $A = 1.7 \times 10^{10}$ and $A = 2.0 \times 10^{10}$, respectively. Figure 9 shows the calculated control pulse for the target packet in Figure 8(a), which is plotted forward in time. Its time- and frequency-resolved spectrum with a parameter of the window function $T_w = 300$ fs is given in Figure 9(b). This pulse includes several frequencies, each of which corresponds to the vibrational components in the target packet. The intensity of each component is determined by the population of the vibrational states included in the packet and their Franck−Condon factors. Corresponding to several transition frequencies, the control pulse has a complicated modulated structure as a function of time (Figure 9a). Its time- and frequency-resolved spectrum in Figure 9(b), however, has a simple form reflecting the vibrational-state distribution given by the solid line in Figure 7(b). The control achievement is quite high, and the absolute square of the overlap integral between the target packet and the optically created packet is 0.982. The control pulse for generating the wave packet in Figure 8(b) is given in Figure 10. This pulse has a similar structure to that in Figure 9. From the time- and frequency resolved spectrum in Figure 10(b), we can see that this pulse is also designed to excite the specific vibrational states which are included in the packet. The absolute overlap integral in this case also has a high value of 0.985. These two numerical examples clearly show that the local control method can be used to design pulses that generate specific wave packets. Since the wave packets treated here are chosen so as to have the shortest or the largest lifetime within given time intervals, we can control the yield of the dissociation product. That is, we can accelerate the predissociation reaction by optically shaping an appropriate target packet.

Here, we would like to point out previous theoretical works[25,26] that treated the lifetime of the predissociating states in NaI and compare those results with our results of variational calculation (eq 24). Using a semiclassical method, Chapman and Child[25] calculated lifetimes including rotational motion. Meier et al.,[26] on the other hand, used a quantum mechanical wave packet calculation, and they determined the lifetime distribution from the energy spectrum of the asymptotic components of the wave packet. These theoretical works were stimulated by the experiments conducted by Zewail's group,[5] in which long time recurrence (∼10 ps) was observed in femtosecond pump−probe signals. Both theoretical calculations succeeded in interpreting the observed spectra in terms of the different distributions in short- and long-lifetime states. Thus our results in Figure 7 are consistent with those of previous works, and our diagonalization method is therefore useful for determining a lifetime distribution.

Finally, we discuss the limitation of our method. Our control scheme consists of two parts. In the first step, we determine the target packet using eq 24, and then we design the control pulse. Strictly speaking, these two processes cannot be separated.

We should determine the best packet for accelerating the predissociation under the influence of a pulse. This naturally leads to a nonlinear equation with respect to the control pulse, which is an optimal control method. On the time scale of several picoseconds, however, it was found in the present study that two-step approximation works well to control the predissociation of NaI. Since the local control method is computationally less expensive than the optimal control method, wave packet shaping with the local control method offers a convenient way to control reaction dynamics such as predissociation of NaI.

4. Summary

We have theoretically studied quantum control of the predissociation of NaI. A local control method was used for designing control pulses that accelerate the predissociation. In section 3A, a 100 fs pump−dump pulse was used to accelerate the predissociation by utilizing a pump−dump control scheme. It was shown that the intrapulse pump−dump process efficiently created the wave packet with a large amplitude in the ground-state potential well. In order to determine the control achievement within a short time, we must consider the dissociation yield after the first passage of the wave packet at the curve crossing. For this purpose, we introduced the dissociation probability, which is defined as the dissociation yield divided by the excited population. The control pulse yielded a dissociation probability about three times higher than that of a transform-limited 60 fs pulse with a central frequency corresponding to the absorption maximum.

In section 3B, a two-step control scheme was used to enhance the predissociation on a longer time scale (several picoseconds). The wave packet prepared by the control pulse at time t_f was chosen so as to maximize the dissociation yield at a given time t_P. For this purpose, we employed a conventional variational procedure to obtain the packet with the shortest lifetime, assuming there is free propagation between time t_f and t_P. This target packet consisted of vibrational states with a short lifetime, and their relative phases were adjusted to enhance the predissociation. The local control method, together with the backward time propagation technique, was applied to the shaping of this target packet. For comparison, we also obtained the control pulse that minimizes the dissociation yield. In both cases, the overlap integrals between the target packet and the optically created packet had a value of more than 98%. Thus, although separate treatment of the two control steps restricts applications, it has been shown that this approximated control scheme efficiently enhances the predissociation reaction on a time scale of several picoseconds.

Acknowledgment. We acknowledge the valuable discussion with Dr. S. Koseki on the transition moment function of NaI. The present work was partly supported by grants for scientific research from the Ministry of Education, Science and Culture, Japan (Nos. 09740511, 10640480, and 10044054), and by a grant for "Development of high-density optical pulse generation and advanced material control techniques" from the Science and Technology Agency, Japan.

References and Notes

(1) Polanyi, J. C.; Zewail, A. H. *Acc. Chem. Res.* **1995**, *28*, 119.
(2) Rosker, M. J.; Rose, T. S.; Zewail, A. H. *Chem. Phys. Lett.* **1988**, *146*, 175.
(3) Engel, V.; Metiu, H.; Almeida, R.; Marcus, R. A.; Zewail, A. H. *Chem. Phys. Lett.* **1988**, *152*, 1.
(4) Rose, T. S.; Rosker, M. J.; Zewail, A. H. *J. Chem. Phys.* **1989**, *91*, 7415.
(5) Cong, P.; Mokhtari, A.; Zewail, A. H. *Chem. Phys. Lett.* **1990**, *172*, 109.
(6) Herek, J. L.; Materny, A.; Zewail, A. H. *Chem. Phys. Lett.* **1994**, *228*, 15.
(7) Taneichi, T.; Kobayashi, T.; Ohtsuki, Y.; Fujimura, Y. *Chem. Phys. Lett.* **1994**, *231*, 50.
(8) Bardeen, C. J.; Che, J.; Wilson, K. R.; Yakovlev, V. V.; Cong, P.; Kohler, B.; Krause, J. L.; Messina, M. *J. Phys. Chem. A* **1997**, *101*, 3815.
(9) Tang, H.; Rice, S. A. *J. Phys. Chem. A* **1997**, *101*, 9587.
(10) Yan, Y.; Gillian, R. E.; Whitnell, R. M.; Wilson, K. R.; Mukamel, S. *J. Phys. Chem.* **1993**, *97*, 2320.
(11) Krause, J. L.; Whitnell, R. M.; Wilson, K. R.; Yan, Y.; Mukamel, S. *J. Chem. Phys.* **1993**, *99*, 6562.
(12) Kohler, B.; Yakovlev, V. V.; Che, J.; Krause, J. L.; Messina, M.; Wilson, K. R.; Schwentner, N.; Whitnell, R. M.; Yan, Y. *Phys. Rev. Lett.* **1995**, *74*, 3360.
(13) Kosloff, R.; Rice, S. A.; Gaspard, P.; Tersigni, S.; Tannor, D. J. *Chem. Phys.* **1989**, *139*, 201.
(14) Kosloff, R.; Hammerich, A. D.; Tannor, D. J. *Phys. Rev. Lett.* **1992**, *69*, 2172.
(15) Bartana, A.; Kosloff, R.; Tannor, D. J. *J. Chem. Phys.* **1993**, *99*, 196.
(16) Tannor, D. J. In *Molecules in Laser Fields*; Bandrauk, A. D., Ed.; Dekker: New York, 1994, Chapter 8.
(17) Sugawara, M.; Fujimura, Y. *J. Chem. Phys.* **1994**, *100*, 5646.
(18) Chen, Y.; Gross, P.; Ramakrishna, V.; Rabitz, H.; Mease, K. *Chem. Phys. Lett.* **1996**, *252*, 447.
(19) Tang, H.; Kosloff, R.; Rice, S. A. *J. Chem. Phys.* **1996**, *104*, 5457.
(20) Ohtsuki, Y.; Yahata, Y.; Kono, H.; Fujimura, Y. *Chem. Phys. Lett.* **1998**, *287*, 627.
(21) Ohtsuki, Y.; Kono, H.; Fujimura, Y. *J. Chem. Phys.* **1998**, *109*, 9318.
(22) Tannor, D. J.; Rice, S. A. *J. Chem. Phys.* **1985**, *83*, 5013.
(23) Tannor, D. J.; Kosloff, R.; Rice, S. A. *J. Chem. Phys.* **1986**, *85*, 5805.
(24) Amstrup, B.; Carlson, R. J.; Matro, A.; Rice, S. A. *J. Phys. Chem.* **1991**, *95*, 8019.
(25) Chapman, S.; Child, M. S. *J. Phys. Chem.* **1991**, *95*, 578.
(26) Meier, Ch.; Engel, V.; Briggs, J. S. *J. Chem. Phys.* **1991**, *95*, 7337.
(27) Gross, P.; Neuhauser, D.; Rabitz, H. *J. Chem. Phys.* **1992**, *96*, 2834.
(28) Peirce, A. P.; Dahleh, M. A.; Rabitz, H. *Phys. Rev. A* **1988**, *37*, 4950.
(29) Shi, S.; Woody, A.; Rabitz, H. *J. Chem. Phys.* **1988**, *88*, 6870.
(30) Jakubets, W.; Manz, J.; Schreiber, H.-J. *Chem. Phys. Lett.* **1990**, *165*, 100.
(31) Shi, S.; Rabitz, H. *J. Chem. Phys.* **1990**, *92*, 364.
(32) Tersigni, S. H.; Gaspard, P.; Rice, S. A. *J. Chem. Phys.* **1990**, *93*, 1670.
(33) Warren, W. S.; Rabitz, H.; Dahleh, M. *Science* **1993**, *259*, 1581.
(34) Zhu, W.; Botina, J.; Rabitz, H. *J. Chem. Phys.* **1998**, *108*, 1953.
(35) Zhu, W.; Rabitz, H. *J. Chem. Phys.* **1998**, *109*, 385.
(36) Ohtsuki, Y.; Zhu, W.; Rabitz, H. *J. Chem. Phys.* **1999**, *110*, 9825.
(37) Alvarellos, J.; Metiu, H. *J. Chem. Phys.* **1988**, *88*, 4957.
(38) Choi, S. E.; Light, J. C. *J. Chem. Phys.* **1989**, *90*, 2593.
(39) Engel, V.; Metiu, H. *J. Chem. Phys.* **1989**, *90*, 6116.
(40) Feit, M. D.; Fleck, J. A., Jr.; Steiger, A. *J. Comput. Phys.* **1982**, *47*, 412.
(41) Kosloff, R. *J. Phys. Chem.* **1988**, *92*, 2087.
(42) Balaknrishnan, N.; Kalyanaraman, C.; Sathyamurthy, N. *Phys. Rep.* **1997**, *280*, 79.
(43) Faist, M. B.; Levine, R. D. *J. Chem. Phys.* **1976**, *64*, 2953.
(44) van Veen, N. J. A.; de Vries, M. S.; Sokol, J. D.; Baller, T.; de Vries, A. E. *Chem Phys.* **1981**, *56*, 81.
(45) Grice, R.; Herschbach, D. R. *Mol. Phys.* **1974**, *27*, 159.
(46) Landau, L. D.; Lifshitz, E. M. *Quantum Mechanics*, Pergamon Press: New York, 1977.
(47) Ruhman, S.; Kosloff, R. *J. Opt. Soc. Am. B* **1990**, *7*, 1748.
(48) Amstrup, B.; Doll, J. D.; Sauerbrey, R. A.; Szabó, G.; Lörincz, A. *Phys. Rev. A* **1993**, *48*, 3830.
(49) Amstrup, B.; Szabó, G.; Sauerbrey, R. A.; Lörincz, A. *Chem. Phys.* **1994**, *188*, 87.
(50) Cao, J.; Bardeen, C. J.; Wilson, K. R. *Phys. Rev. Lett.* **1998**, *80*, 1406.
(51) Cao, J.; Che, J.; Wilson, K. R. *J. Phys. Chem. A* **1998**, *102*, 4284.
(52) For more rigorous classical−mechanical treatment, see, e.g., Bersohn, R.; Zewail, A. H. *Ber. Bunsen-Ges. Phys. Chem.* **1988**, *92*, 373.
(53) Bardeen, C. J.; Wang, Q.; Shank, C. V. *Phys. Rev. Lett.* **1995**, *75*, 3410.
(54) Cerullo, G.; Bardeen, C. J.; Wang, Q.; Shank, C. V. *Chem. Phys. Lett.* **1996**, *262*, 362.